

Experimental Determination of the Phase Diagram of the CaO-SiO₂-5 pctMgO-10 pctAl₂O₃-TiO₂ System



JUNJIE SHI, LIFENG SUN, BO ZHANG, XUQIANG LIU, JIYU QIU,
ZHAOYUN WANG, and MAOFA JIANG

Ti-bearing CaO-SiO₂-MgO-Al₂O₃-TiO₂ slags are important for the smelting of vanadium-titanium bearing magnetite. In the current study, the pseudo-melting temperatures were determined by the single-hot thermocouple technique for the specified content of 5 to 25 pct TiO₂ in the CaO-SiO₂-5 pctMgO-10 pctAl₂O₃-TiO₂ phase diagram system. The 1573 K to 1773 K (1300 °C to 1500 °C) liquidus lines were first calculated based on the pseudo-melting temperatures according to thermodynamic equations in the specific primary crystal field. The phase equilibria at 1573 K (1300 °C) were determined experimentally using the high-temperature equilibrium and quench method followed by X-ray fluorescence, X-ray diffraction, scanning electron microscope, and energy dispersive X-ray spectroscopy analysis; the liquid phase, melilite solid solution phase (C₂MS₂C₂AS)_{ss}, and perovskite phase of CaO·TiO₂ were found. Therefore, the phase diagram was constructed for the specified region of the CaO-SiO₂-5 pctMgO-10 pctAl₂O₃-TiO₂ system.

DOI: 10.1007/s11663-015-0527-3

© The Minerals, Metals & Materials Society and ASM International 2015

I. INTRODUCTION

THE Ti-bearing system, described by the CaO-SiO₂-MgO-Al₂O₃-TiO₂ system, forms the basis for a number of metallurgical slag systems, especially for smelting of vanadium-titanium bearing magnetite in blast furnace.^[1-3] The presentation of TiO₂ has been considered as the cause of the “gumminess,” which leads to the malfunctioning of blast furnace. Characterization of Ti-bearing slag system is critical for facilitating improvements in the development and optimization of processes related to the smelting of vanadium-titanium bearing magnetite. But the phase relationship of Ti-bearing system is difficult to study because of the high temperature required and the complex reactions between different components.

The liquidus and phase relations of the Ti-bearing slag system have been studied in part by several authors,^[4-9] and the phase diagram of the CaO-SiO₂-TiO₂ ternary system was first completely investigated by DeVries *et al.*^[5] Based on the phase diagram of the CaO-SiO₂-TiO₂ system, the effect of adding MgO, Al₂O₃ and TiO₂ on the liquidus temperature of Ti-bearing slags have been investigated. It was reported by Fine *et al.*^[6] that TiO₂ addition increases the liquidus temperature of CaO-SiO₂-MgO-Al₂O₃ slags, while Ohon *et al.*^[7] reported that the liquidus temperature was

decreased with the increase of TiO₂. Osborn *et al.*^[8] studied the effect on liquidus temperatures of adding TiO₂ to CaO-SiO₂-MgO-Al₂O₃ compositions on air atmosphere; the results indicated that the liquidus temperatures were not greatly influenced. The phase equilibrium at reducing conditions was studied by Zhao *et al.*^[9] and the melting temperatures were described as a function of basicity and the TiO_x concentration. However, the phase relations of the CaO-SiO₂-TiO₂ system with the additions of Al₂O₃ and MgO remain unclear, and the lack of thermodynamic information^[10-12] for the liquidus temperature and phase relations has severely hindered the development and application of the above mentioned system.

In the current study, the liquidus and phase relations of the CaO-SiO₂-5 pctMgO-10 pctAl₂O₃-TiO₂ system were studied systematically. The single-hot thermocouple technique (SHTT) was used to determine pseudo-melting temperatures of the complex slags, and the liquidus was calculated based on the pseudo-melting temperatures according to the thermodynamic equations. Coupled with a small number of high-temperature equilibria experiments at 1573 K (1300 °C), the phase diagram for the specific region of the CaO-SiO₂-5 pctMgO-10 pctAl₂O₃-TiO₂ system could be constructed. The results of the current work can also be helpful for studying the comprehensive utilization of Ti-bearing furnace slag and the development of thermodynamic databases.

JUNJIE SHI and JIYU QIU, Doctoral Candidates, XUQIANG LIU and ZHAOYUN WANG, Master Candidates, BO ZHANG, Lecturer, LIFENG SUN, Associate Professor, and MAOFA JIANG, Professor, are with the Key Laboratory for Ecological Metallurgy of Multimetallic Ores (Ministry of Education), Northeastern University, Shenyang 110819, P.R. China. Contact e-mail: sunlf@smm.neu.edu.cn

Manuscript submitted May 06, 2015.

Article published online November 30, 2015.

II. EXPERIMENT

A. Sample Preparation

Reagent grade oxides powders of CaO (99.99 wt pct pure), SiO₂ (99.99 wt pct pure), MgO (99.99 wt pct

Table I. The Comparison of Designed and XRF Measured Compositions of Ti-Bearing Slags, Mass Pct

Slag No.		w(CaO)/w(SiO ₂)	CaO	SiO ₂	MgO	Al ₂ O ₃	TiO ₂
M1	Designed	0.88	37.10	42.34	4.84	10.57	5.15
	XRF	0.80	35.56	44.44	5.00	10.00	5.00
M2	Designed	1.05	40.46	38.59	5.28	10.30	5.20
	XRF	1.00	40.00	40.00	5.00	10.00	5.00
M3	Designed	1.19	43.18	36.18	5.38	10.26	4.99
	XRF	1.20	43.64	36.36	5.00	10.00	5.00
M4	Designed	1.31	45.13	34.49	5.19	9.64	5.55
	XRF	1.17	43.19	36.81	5.00	10.00	5.00
M5	Designed	1.37	46.13	33.70	4.99	9.88	5.30
	XRF	1.34	45.81	34.19	5.00	10.00	5.00
M6	Designed	1.42	47.06	33.15	4.96	9.74	5.09
	XRF	1.36	46.10	33.90	5.00	10.00	5.00
M7	Designed	1.52	48.42	31.82	4.96	9.71	5.09
	XRF	1.50	48.00	32.00	5.00	10.00	5.00
M8	Designed	0.76	33.82	44.49	4.78	9.56	7.35
	XRF	0.80	34.44	43.06	5.00	10.00	7.50
M9	Designed	0.90	37.27	41.43	4.82	9.63	6.85
	XRF	1.00	38.75	38.75	5.00	10.00	7.50
M10	Designed	1.16	41.94	36.10	5.07	10.14	6.75
	XRF	1.07	40.06	37.44	5.00	10.00	7.50
M11	Designed	1.28	44.41	34.60	4.75	9.49	6.75
	XRF	1.14	41.29	36.21	5.00	10.00	7.50
M12	Designed	1.48	46.74	31.55	4.97	9.94	6.80
	XRF	1.30	43.80	33.70	5.00	10.00	7.50
M13	Designed	0.79	30.03	38.12	5.03	10.06	16.76
	XRF	0.80	31.11	38.89	5.00	10.00	15.00
M14	Designed	0.89	31.80	35.88	5.16	10.31	16.85
	XRF	0.87	32.57	37.43	5.00	10.00	15.00
M15	Designed	0.98	33.99	34.54	5.11	10.23	16.12
	XRF	0.94	33.92	36.08	5.00	10.00	15.00
M16	Designed	1.05	35.54	33.71	5.00	10.01	15.75
	XRF	1.00	35.00	35.00	5.00	10.00	15.00
M17	Designed	1.31	39.98	30.43	4.87	9.75	14.96
	XRF	1.20	38.18	31.82	5.00	10.00	15.00
M18	Designed	1.46	42.04	28.78	4.99	9.97	14.22
	XRF	1.30	39.57	30.43	5.00	10.00	15.00
M19	Designed	1.72	45.49	26.48	4.71	9.42	13.92
	XRF	1.50	42.00	28.00	5.00	10.00	15.00
M20	Designed	0.79	28.13	35.58	5.06	10.12	21.10
	XRF	0.80	28.89	36.11	5.00	10.00	20.00
M21	Designed	0.88	29.45	33.51	5.03	10.07	21.94
	XRF	0.87	30.24	34.76	5.00	10.00	20.00
M22	Designed	0.96	30.95	32.29	5.01	10.02	21.74
	XRF	0.94	31.49	33.51	5.00	10.00	20.00
M23	Designed	1.01	31.88	31.60	5.04	10.09	21.39
	XRF	1.00	32.50	32.50	5.00	10.00	20.00
M24	Designed	1.24	35.70	28.71	5.03	10.05	20.51
	XRF	1.20	35.45	29.55	5.00	10.00	20.00
M25	Designed	1.38	37.73	27.44	5.07	10.14	19.61
	XRF	1.30	36.74	28.26	5.00	10.00	20.00
M26	Designed	1.52	40.26	26.43	4.90	9.80	18.61
	XRF	1.40	37.92	27.08	5.00	10.00	20.00
M27	Designed	0.82	26.17	31.94	5.09	10.19	26.61
	XRF	0.80	26.67	33.33	5.00	10.00	25.00
M28	Designed	0.91	27.87	30.58	5.11	10.23	26.22
	XRF	0.90	28.42	31.58	5.00	10.00	25.00
M29	Designed	1.03	29.68	28.93	5.13	10.27	25.99
	XRF	1.00	30.00	30.00	5.00	10.00	25.00
M30	Designed	1.25	33.22	26.64	5.21	10.42	24.52
	XRF	1.20	32.73	27.27	5.00	10.00	25.00
M31	Designed	1.33	35.20	26.47	5.29	10.58	22.46
	XRF	1.30	33.91	26.09	5.00	10.00	25.00

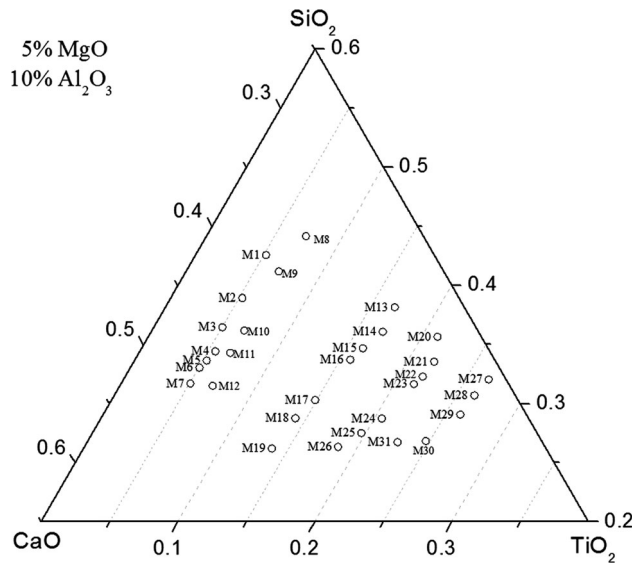


Fig. 1—The projection of pre-melt compositions on CaO-SiO₂-5 pctMgO-10 pctAl₂O₃-TiO₂ phase diagram, mass pct.

pure), Al₂O₃ (99.99 wt pct pure), and TiO₂ (99.99 wt pct pure) were employed to synthesize the slags, which were calcined at 1273 K (1000 °C) for 4 hours to evaporate the moisture and impurities, respectively, and carefully weighted, fully mixed and pre-melted in Ar atmosphere using vertical MoSi₂ furnace. The mixtures were placed inside platinum crucibles which were suspended by platinum wire inside the hot zone of the furnace at 1923 K (1650 °C) for 2 hours to completely homogenize the slags. The samples were then quenched into ice water, dried, crushed, and grinded to 200 meshes for further utilization. The composition of the quenched slags was analyzed by X-Ray fluorescence (XRF), as listed in Table I. In the preparation of the samples, all the compositions have been aimed at in the 10 pct Al₂O₃ and 5 pct MgO section. However, none of the experimental points lies exactly on the 10 pct Al₂O₃ and 5 pct MgO section in CaO-SiO₂-MgO-Al₂O₃-TiO₂ system. In order to visualize the composition of the samples, the normalization was done according to Gran *et al.*^[13] with the following procedure: the Al₂O₃ and MgO content were adjusted to 10 and 5 pct, whereas the compositions of the rest of the components are normalized in proportion to their original fractions with their sum being 85 pct. The projection of the pre-melted composition on the CaO-SiO₂-5 pctMgO-10 pctAl₂O₃-TiO₂ pseudo-ternary phase diagram is shown in Figure 1.

B. Pseudo-Melting Temperature Determination

The SHTT technique was used to measure the pseudo-melting temperature of the slags in the current experiments. Using the SHTT technique to measure the temperature has been proven as an effective method according to previous work.^[7] The principle of SHTT technique has been described in detail^[14–16] and is briefly summarized in this study. A B-type thermocouple (0.2 mm in diameter) was used during heating to measure the

temperature simultaneously. A microscope equipped with a video camera was applied to *in-situ* observe and record the images of slag, which were sent to a computer and a video cassette recorder. The heating process was controlled by a computer program.

The following method, as illustrated in Figure 2, was used for the judgements of the melting temperatures. During the experiments, approximately 10 mg slag was mounted on the tip of thermocouple and heated rapidly at the rate of 5 to 10 K/s (5 to 10 °C/s) to a point 50 K to 200 K (50 °C to 200 °C) below the approximate melting temperature, as shown in Figure 2(a). Since the temperature was measured most accurately at the tip of the thermocouple, the part of the slag surrounding the tip of the thermocouple was chosen for observing and measuring, as shown in the circular arc area in Figures 2(a) and (b). It was clearly seen that the slag was completely solid in Figure 2(a). Then, the slag was heated continuously at the very slow rate of 0.1 K/second (0.1 °C/second) to the temperature shown in Figure 2(b), at which the slag close to the tip of the thermocouple first became fluid and transparent, while the slag far from the thermocouple tip was still solid, which meant the slag around the thermocouple tip had already become liquid. The temperature of the state in Figure 2(b) was found reproducible and could be taken as the melting temperature of the slag, which is called pseudo-melting temperature in this paper. As heating continued, the remaining slag became liquid because of heat transfer in Figure 2(c). The whole melting process was recorded as a video file and the pseudo-melting temperature was then obtained.

Each measurement was performed at least three times to verify reproducibility. At the beginning of each measurement, the B-type thermocouple was calibrated against pure NaF and CaF₂ to ensure the temperature accuracy within ±1 K (1 °C).

C. Equilibration Experiments

The vertical furnace used for the pre-melt was used for the equilibria experiments. The furnace temperature was monitored by a B-type thermocouple placed next to the samples with an overall temperature accuracy estimated to be ±2 K (2 °C). The platinum crucibles, holding specific oxide mixtures, were suspended by platinum wire (0.5mm diameter) in the even temperature zone of the furnace. All samples were pre-melted before equilibration at 1923 K (1650 °C) for 1 to 3 hours, after which the furnace temperature was cooled to the equilibration temperature; an equilibration time of 24 hours, based on experiences reported by previous authors,^[17–19] was used to guarantee equilibrium had been reached. Argon gas was passed through the furnace during the entire experiment to avoid moisture and other potential contamination sources. Quenching was made by dropping the sample directly into ice water placed under the furnace, and the vertical tube furnace would allow the sample to be quenched within a second, retaining the phases present at the equilibrium temperature. Samples were then dried and mounted in epoxy resin and polished for analysis. X-ray fluorescence

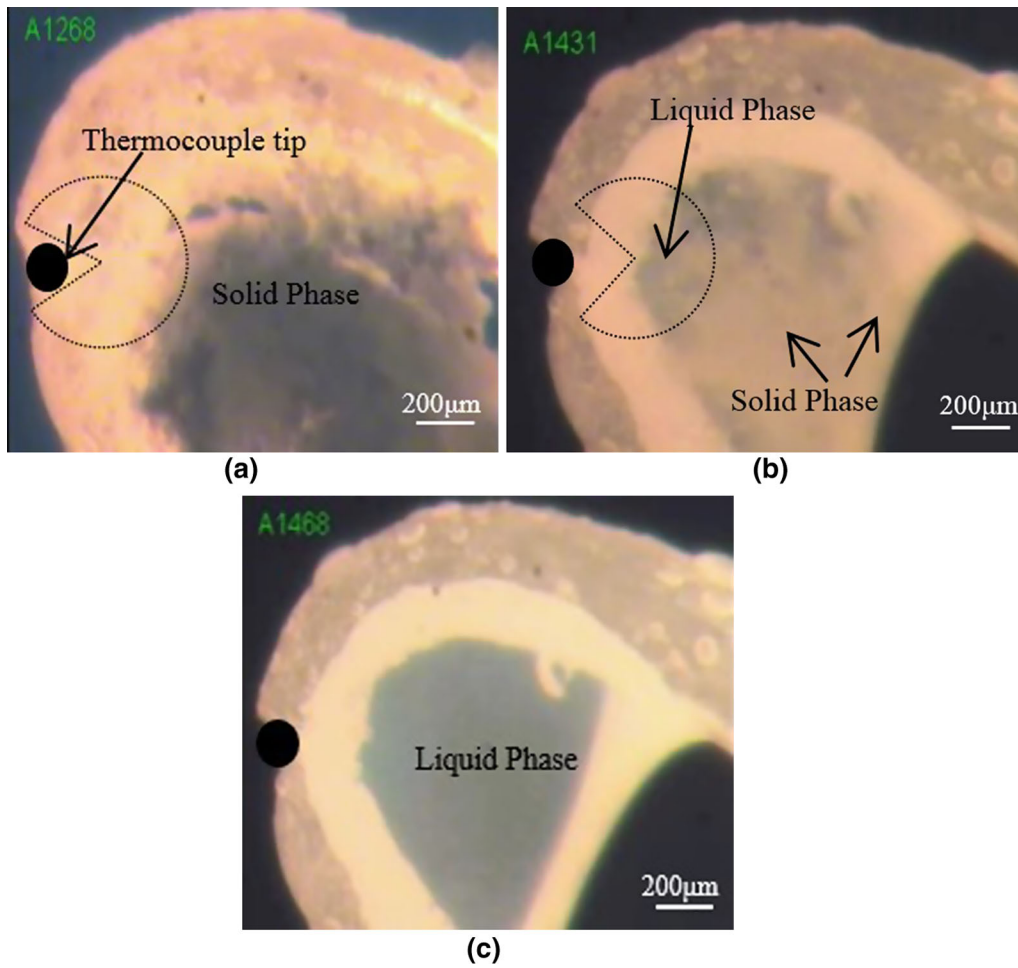


Fig. 2—The judgement standard of pseudo-melting temperature by the SHTT method (a) 1541 K (1268 °C) (b) 1704 K (1431 °C) (c) 1741 K (1468 °C).

(XRF), X-ray diffraction (XRD), scanning electron microscope (SEM), and energy dispersive X-ray spectroscopy (EDX) were used to identify the coexisting phases and analyze the composition of each sample.

For obtaining more accurate phase compositions, the partition of elements in each phase were examined several times in different areas of the sample, and the average concentration of each phase was determined through repeated analyses to overcome the roughness of EDS.

III. RESULTS AND DISCUSSION

A. Results of Pseudo-Melting Temperatures

The pseudo-melting temperatures are listed in Table II, and the average of T_1 , T_2 , and T_3 was chosen as the pseudo-melting temperature T .

The pseudo-melting temperatures were compared with the existing phase diagram^[4,8] which was constructed by the traditional high-temperature equilibrium and quench method, as shown in Figure 3. The pseudo-melting temperatures measured by SHTT agreed

fairly well with the liquidus lines in the phase diagram. It could also find that the pseudo-melting temperatures change gradually with the increase of the basicity of $w(\text{CaO})/w(\text{SiO}_2)$, as shown in Figure 4. The temperature increases from 1531 K to 1755 K (1258 °C to 1482 °C) when the basicity of $w(\text{CaO})/w(\text{SiO}_2)$ increases from 0.83 to 1.52 with a TiO_2 content of 5 pct. Furthermore, the relationship of temperature with $w(\text{CaO})/w(\text{SiO}_2)$ showed three different segments in different areas, namely M1-M3, M3-M5, and M5-M7. The reason for the different slopes in the three segments will be discussed in detail in the following discussion, and the change is similar when the content of TiO_2 is fixed at other values such as 7.5, 15, 20, and 25 pct.

B. Construction of the Liquidus Lines

The gradient change in different areas could be explained by thermodynamic equations, which could be deduced with reference to the isothermal phase diagram in Figure 5. In the primary phase of B, the point M located on the liquidus line represents the equilibrium of solid B with liquid.

Table II. The Determined Pseudo-Melting Temperatures and Calculated Temperatures of Ti-Bearing Slags, K

NO.	w(CaO)/w(SiO ₂)	w(TiO ₂)	T ₁ , K	T ₂ , K	T ₃ , K	T, K	T _{cal.} , K	ΔT, K
M1	0.88	5.15	1524	1522	1524	1523	1523	0
M2	1.05	5.20	1569	1575	1571	1572	1577	5
M3	1.19	4.99	1613	1617	1621	1617	1617	0
M4	1.31	5.55	1632	1635	1634	1634	1638	4
M5	1.37	5.30	1647	1649	1651	1649	1649	0
M6	1.42	5.09	1683	1682	1681	1682	1684	2
M7	1.52	5.09	1755	1754	1757	1755	1756	1
M8	0.76	7.35	1562	1555	1557	1558	1559	1
M9	0.90	6.85	1581	1577	1576	1578	1576	-2
M10	1.16	6.75	1603	1600	1602	1602	1602	0
M11	1.28	6.75	1624	1626	1626	1625	1625	0
M12	1.48	6.80	1663	1660	1663	1662	1662	0
M13	0.79	16.76	1561	1564	1566	1564	1562	-2
M14	0.89	16.85	1603	1602	1607	1604	1608	4
M15	0.98	16.12	1651	1650	1649	1650	1649	-1
M16	1.05	15.75	1667	1669	1670	1669	1670	0
M17	1.31	14.96	1742	1739	1740	1740	1740	0
M18	1.46	14.22	1758	1755	1756	1756	1752	-4
M19	1.72	13.92	1766	1768	1766	1767	1768	1
M20	0.79	21.10	1576	1576	1573	1575	1572	-3
M21	0.88	21.94	1614	1612	1611	1612	1619	7
M22	0.96	21.74	1662	1663	1660	1662	1661	-1
M23	1.01	21.39	1679	1673	1675	1676	1677	0
M24	1.24	20.51	1748	1748	1750	1749	1749	0
M25	1.38	19.61	1769	1768	1770	1769	1769	0
M26	1.52	18.61	1787	1789	1786	1787	1787	0
M27	0.82	26.61	1579	1580	1582	1580	1579	-1
M28	0.91	26.22	1621	1619	1622	1621	1617	-4
M29	1.03	25.99	1661	1656	1659	1659	1665	6
M30	1.25	24.52	1746	1751	1746	1748	1748	0
M31	1.33	22.46	1778	1780	1777	1778	1776	-2

$$T = (T_1 + T_2 + T_3)/3; T_{cal.} \text{ means the calculated temperature; } \Delta T = T_{cal.} - T.$$

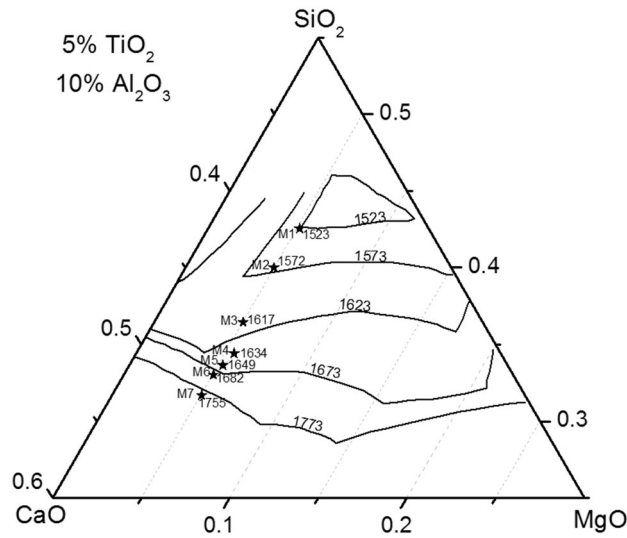


Fig. 3—Comparison of the experimental datas from present results with the existing phase diagram (K).

When the liquid slag is taken as the ideal solution, from the equal of chemical potential, Eq. [1] can be deduced.

$$u_{B(l)} = u_{B(s)} \quad [1]$$

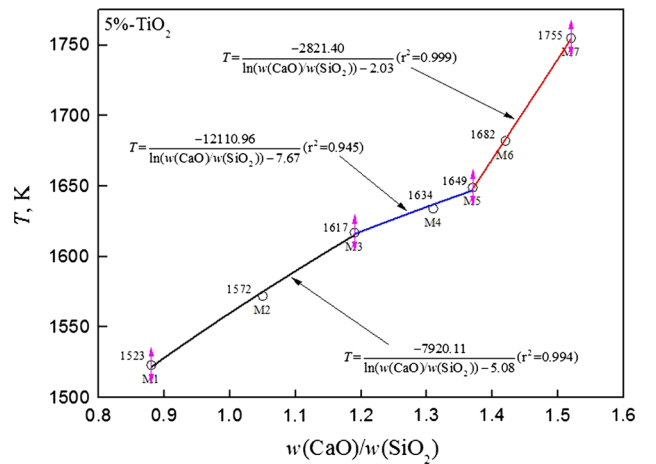


Fig. 4—The relation of temperature *T* with basicity *w*(CaO)/*w*(SiO₂) for 5 pct content of TiO₂.

The terms $u_{B(l)}$ and $u_{B(s)}$ in Eq. [1] are the chemical potential of liquid B and solid B, respectively. Taking pure solid oxide and pure liquid as the standard state, the chemical potential of solid B and liquid B can be expressed in Eqs. [2] and [3], respectively:

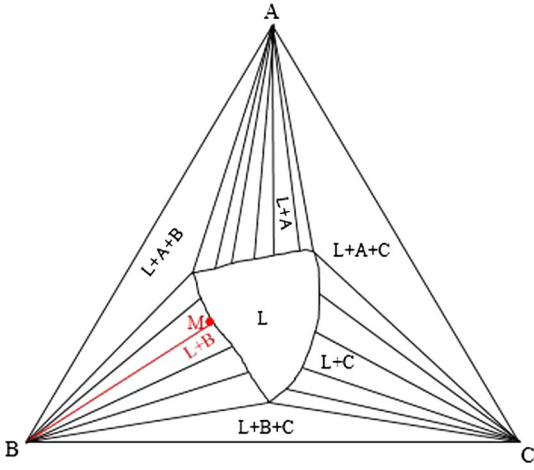


Fig. 5—Schematic of isothermal A-B-C phase diagram at temperature of T .

$$u_{B(l)} = u_{B(l)}^\theta + RT \ln x_{B(l)} = G_{B(l)}^\theta + RT \ln x_{B(l)}, \quad [2]$$

$$u_{B(s)} = u_{B(s)}^\theta + RT \ln x_{B(s)} = G_{B(s)}^\theta + RT \ln x_{B(s)}. \quad [3]$$

The term R is the gas constant. T is the isothermal temperature; $x_{B(l)}$ and $x_{B(s)}$ are the mass fractions of B in liquid and solid, respectively. The value of $x_{B(s)}$ is 1 when the pure solid oxide is taken as the standard state. When Eqs. [2] and [3] are combined with Eq. [4] and the Gibbs–Helmholtz equation in Eq. [5]

$$\Delta G_{B(\text{fus})}^\theta = G_{B(l)}^\theta - G_{B(s)}^\theta, \quad [4]$$

$$\Delta G_{B(\text{fus})}^\theta = \Delta H_{B(\text{fus})}^\theta \left(1 - \frac{T}{T_m}\right), \quad [5]$$

the following Eq. [6] can be deduced:

$$x_{B(l)} = \exp \left[-\frac{\Delta H_{B(\text{fus})}^\theta}{R} \frac{1}{T} + \frac{\Delta H_{B(\text{fus})}^\theta}{RT_m} \right]. \quad [6]$$

The terms $T_m, \Delta H_{B(\text{fus})}^\theta$ in Eq. [6] are the pseudo-melting temperature and molar Gibbs energy of pure solid B , respectively. As the value of R , T_m and $\Delta H_{B(\text{fus})}^\theta$ are almost constant and the term $x_{B(l)}$ stands for the variables of composition such as $w(\text{TiO}_2)$ and $w(\text{CaO})/w(\text{SiO}_2)$, which could be simplified as x . Then Eq. [6] can be simplified as:

$$x = \exp \left(\frac{a}{T} + b \right). \quad [7]$$

Equation [7] can be further simplified for discussing the relation of T with composition x , as shown in Eq. [8]:

$$T = \frac{a}{\ln x - b}. \quad [8]$$

Equation [8] can be used to fit the relation between T and x in the specific primary crystal field of substance B .

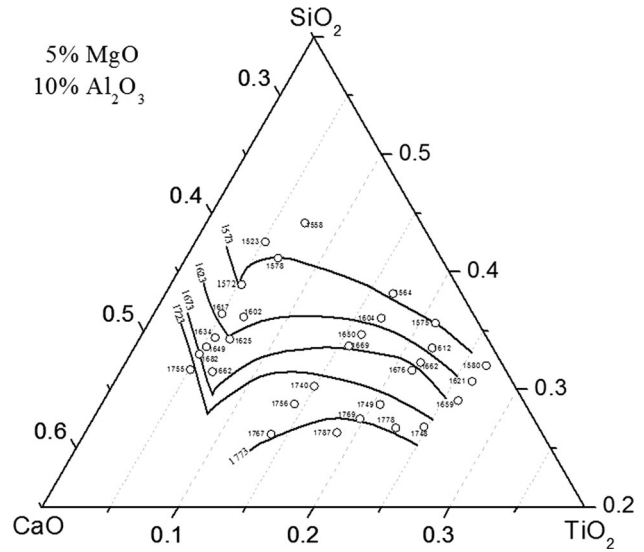


Fig. 6—The 1573 K to 1773 K (1300 °C to 1500 °C) liquidus lines calculated based on the pseudo-melting temperature, K.

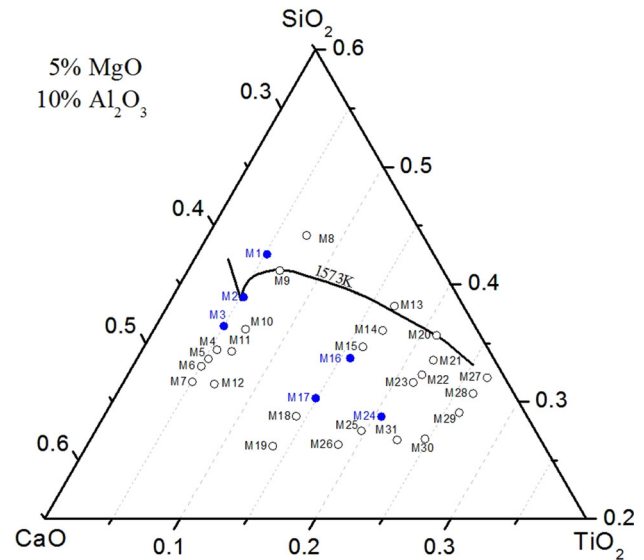


Fig. 7—Selected equilibrium points for CaO-SiO₂-5 pct MgO-10 pct Al₂O₃-TiO₂ at 1573 K (1300 °C).

The notation a and b stands for $a = -\frac{\Delta H_{B(\text{fus})}^\theta}{R}$ and $b = \frac{\Delta H_{B(\text{fus})}^\theta}{RT_m}$, respectively, which can be taken as constant and can be determined through regression of the experimentally measured pseudo-melting temperature.

In the actual fitting process for an unknown phase diagram system, such as the CaO-SiO₂-5 pct MgO-10 pct Al₂O₃-TiO₂ system reported in this paper, the experimental points within the same primary crystal field remain uncertain before the regression. Under this circumstance, the following principle is adopted to obtain the optimal fitting: the temperature change with the basicity of $w(\text{CaO})/w(\text{SiO}_2)$ at different TiO₂ content is plotted first and then the character of the gradient is analyzed, after which the points with the same gradient

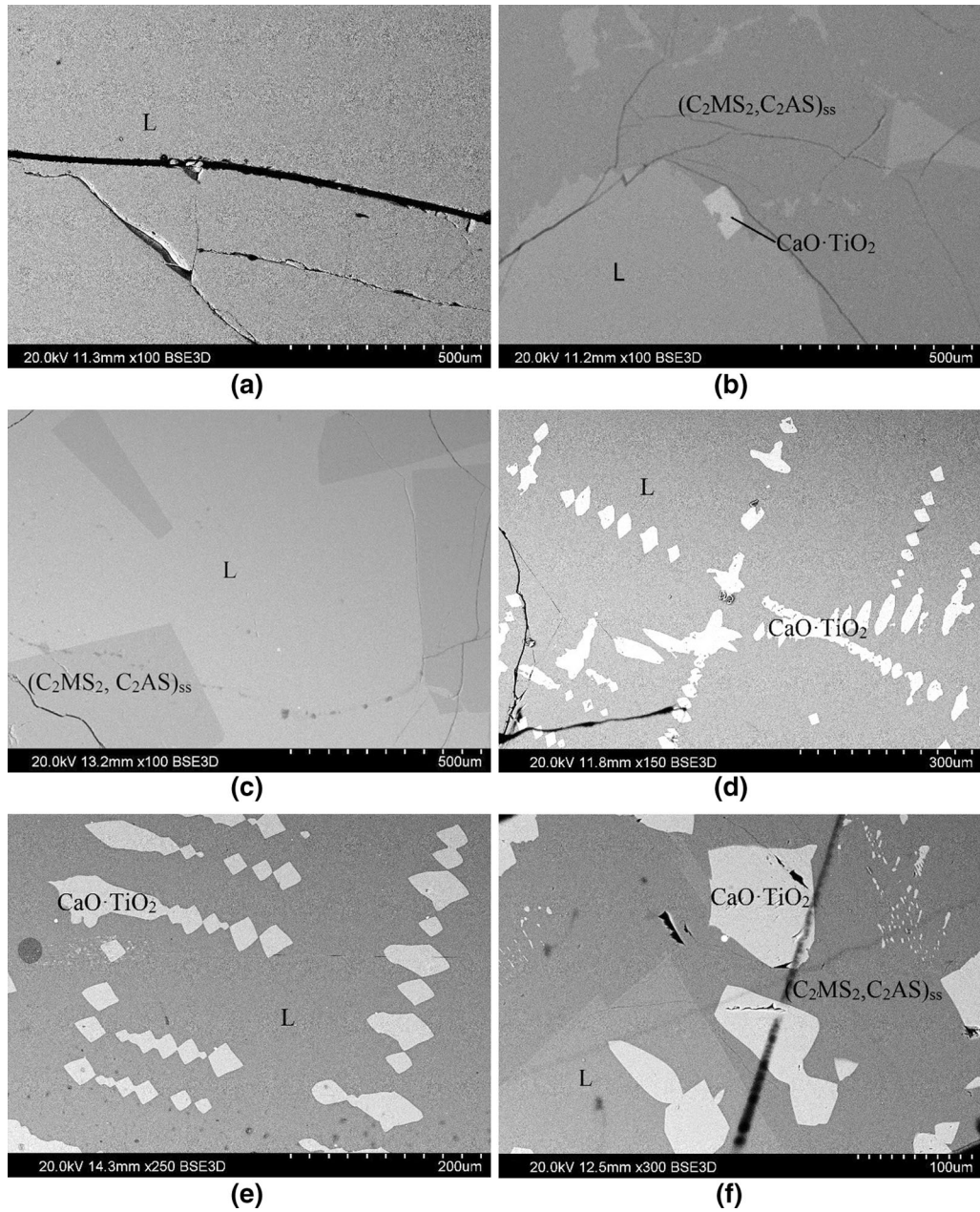


Fig. 8—SEM microphotographs of equilibria phases under 1573 K (1300 °C) (a) M1 (b) M3 (c) M3 (d) M16 (e) M24 (f) M17.

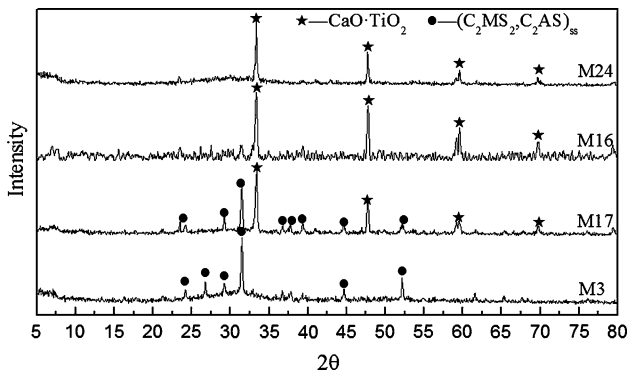


Fig. 9—The XRD results of equilibration phase.

will be regressed together. Taking Figure 4 as an illustration, the temperature change with $w(\text{CaO})/ w(\text{SiO}_2)$ shows three different gradients at 5 pct TiO_2 , then Eq. [8] is applied to each gradient and the fitting effect is good as shown in Figure 4. The fitting process at other contents of TiO_2 is done in the same way. The temperatures at the same composition calculated by the regressive equations agree well with the experimentally determined temperature, which can be found in Table II.

Using the regressive equations, the liquidus lines of 1573 K to 1773 K (1300 °C to 1500 °C) of the $\text{CaO-SiO}_2\text{-5 pctMgO-10 pctAl}_2\text{O}_3\text{-TiO}_2$ system are calculated, as shown in Figure 6. The shapes of liquidus lines are similar to each other from 1573 K to 1723 K

(1300 °C to 1450 °C), and a spinodal is clearly observed for each liquidus line, in which the composition of the spinodal moves to higher basicity and higher content of TiO₂ with temperature increases.

C. Estimation of Equilibrium Phase

In order to clarify the phase relations in the CaO-SiO₂-5 pct MgO-10 pct Al₂O₃-TiO₂ system, six samples were selected for equilibration at 1573 K (1300 °C) to detect the primary crystal phase, as the solid points in Figure 7. The SEM micrographs and XRD results of the samples are shown in Figures 8 and 9, respectively, and the composition of the phase in the quenched samples, as measured by EDS, is presented in Table III.

Sample M1 in Figure 8(a) presents as single phase at 1573 K (1300 °C) and the composition of this single phase in Table III is close to the initial composition of the pre-melt composition of M1, which means M1 was liquid at 1573 K (1300 °C). On the other way, this result is consistent with the pseudo-melting temperature determined in Table II, as the pseudo-melting temperature of M1 is 1523 K (1250 °C). The situation of M2 is similar with M1 and the equilibrium phase is liquid too.

As for sample M3, it can be concluded from XRD result in Figure 9 that only the crystal of melilite solid solution of (C₂MS₂,C₂AS)_{ss} with dark gray in Figure 8(b) is detected. But the EDS result in Table III suggests that the perovskite phase of CaO·TiO₂ with white block shape in Figure 8(b) exists in sample M3. In order to confirm the equilibria phases exist at 1573 K (1300 °C), a new equilibrium experiment at the same condition for sample M3 at 1573 K (1300 °C) is carried out, and the equilibria phases are detected by SEM, as shown in Figure 8(c), only the melilite solid solution phase is found to coexist with the liquid phase. Therefore, the CaO·TiO₂ phase is confirmed as precipitations during the cooling process due to the finite quenching speed, and the equilibria phases of M3 are melilite solid solution phase ((C₂MS₂,C₂AS)_{ss}) and liquid phase, in which the light gray phase is liquid

phase. It is worth to mention that it seems an eutectic reaction of L → (C₂MS₂, C₂AS)_{ss} + CaO·TiO₂ will occur near the composition of M3 and near 1575 K (1300 °C).

Base on the same principle, the equilibria phases of sample M16 and sample M24 are confirmed as liquid coexist with perovskite phase(CaO·TiO₂), while sample M17 is identified as three-phase equilibrium with liquid coexist with CaO·TiO₂ and (C₂MS₂,C₂AS)_{ss}. The compositions of liquidus phase are compared with the calculated 1573 K (1300 °C) liquidus line on the pseudo-ternary CaO-SiO₂-TiO₂-5 pctMgO-10 pctAl₂O₃ phase diagram, which could be found in Figure 10. As can be seen, the liquidus composition of M16 and M24 are quite close to the 1573 K (1300 °C) liquidus line, which means the results of high-temperature equilibria experiments are well in accordance with the liquidus line

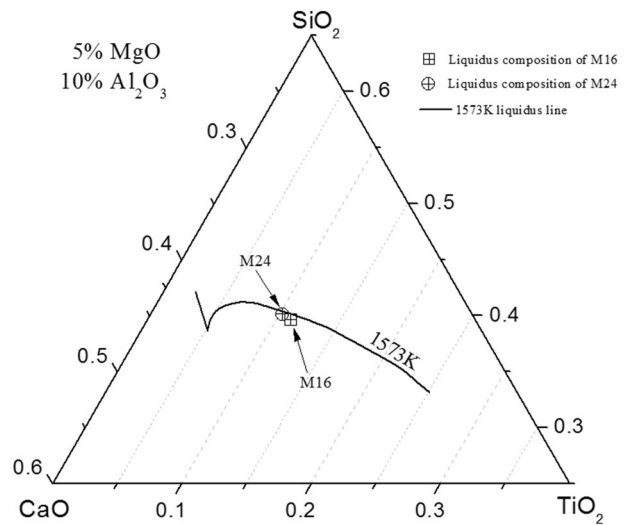


Fig. 10—Comparison of experimental liquid composition with calculated 1573 K (1300 °C) liquidus line for samples M16 and M24.

Table III. Experimental Determined Phase Compositions of CaO-SiO₂-5 pctMgO-10 pctAl₂O₃-TiO₂ system at 1573 K (1300 °C)

Sample No.	Contrast in the SEM Microphotograph	Phase	Composition, Mass pct				
			CaO	SiO ₂	MgO	Al ₂ O ₃	TiO ₂
M1	gray	L	35.69	45.32	5.07	9.00	4.92
M2	gray	L	40.65	40.39	4.68	9.17	5.11
M3	light gray	L	46.16	37.60	3.33	6.85	6.07
	dark gray	(C ₂ MS ₂ ,C ₂ AS) _{ss}	42.96	37.72	8.15	11.17	0.00
	white	CT	43.11	0.00	0.00	0.00	56.89
M16	gray	L	34.48	39.94	5.26	9.19	11.14
	white	CT	40.05	0.00	0.00	0.00	59.95
M24	gray	L	33.80	39.15	6.18	10.92	9.94
	white	CT	41.92	0.00	0.00	0.00	58.08
M17	light gray	L	35.39	38.11	5.63	12.84	8.04
	white	CT	41.72	0.00	0.00	0.00	58.28
	dark gray	(C ₂ MS ₂ ,C ₂ AS) _{ss}	42.97	36.50	7.76	12.77	0.00

L: Liquid, C: CaO, M: MgO, S: SiO₂, A: Al₂O₃, T: TiO₂.

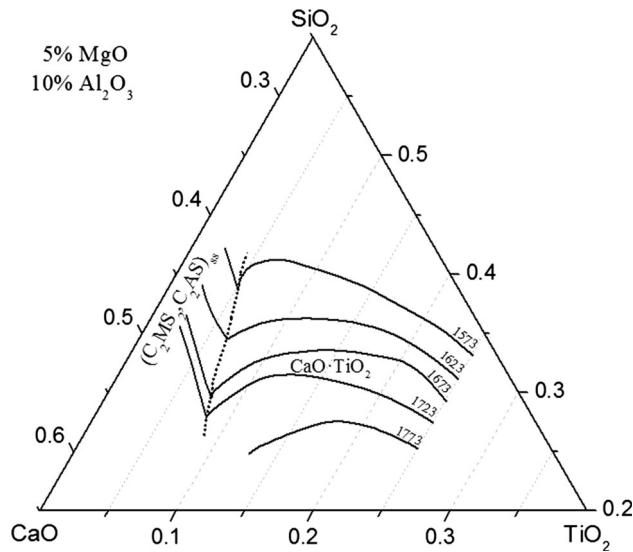


Fig. 11—The phase diagram for the specific area of CaO-SiO₂-5 pctMgO-10 pctAl₂O₃-TiO₂ system.

calculated based on the pseudo-melting temperature measured by SHTT.

D. Presentation of the Phase Diagram

Coupling with the liquidus lines calculated in Figure 6 and the equilibria phases at 1573 K (1300 °C) confirmed above; the phase diagram at specific area for CaO-SiO₂-5 pctMgO-10 pct Al₂O₃-TiO₂ system is constructed in Figure 11. The dotted line is the predicted phase boundary line and the left area is dominated by the melilite solid solution phase of (C₂MS₂, C₂AS)_{ss}, while the right area is dominated by the perovskite phase of CaO·TiO₂.

IV. CONCLUSION

The coupling of SHTT/high-temperature equilibrium experimental approach has been developed and applied to investigate the pseudo-melting temperature and the phase relations for 5 to 25 pct of TiO₂ in the CaO-SiO₂-5 pctMgO-10 pctAl₂O₃-TiO₂ system. The 1573 K to 1773 K (1300 °C to 1500 °C) liquidus lines were first calculated based on the pseudo-melting temperature according to thermodynamic equations in the specific primary crystal field. The liquid phase coexistent with (C₂MS₂, C₂AS)_{ss} solid solution phase and CaO·TiO₂ phase was found, and the phase diagram was constructed for the specified region of the CaO-SiO₂-5 pctMgO-10 pctAl₂O₃-TiO₂ system based on the

liquidus lines and the equilibria phases. It is worth to mention that it is a good attempt to use the coupled SHTT and high-temperature equilibrium technique to construct the phase diagram in this system at conditions relevant to industrial processes, such as, smelting of vanadium-titanium bearing magnetite.

ACKNOWLEDGMENTS

This work was financially supported by the National Natural Science Foundation of China (Nos. 51104039 and 51304042), Scientific Research Fund of Liaoning Provincial Education Department (No. L2013114), Programs of Liaoning province for Science and Technology Development (No. 2012221013), and the Fundamental Research Funds for the Central Universities of China (N130602002).

REFERENCES

1. P.M Guo and P. Zhao: *Iron Steel Vanadium Titan.*, 2005, vol. 26 (2), pp. 5–10.
2. W. Zhang, L. Zhang, J.H. Zhang, and N.X. Ind: *Eng. Chem. Res.*, 2012, vol. 51, pp. 12294–98.
3. H.W. Ma: *Industrial Minerals and Rocks*, 3rd ed., Chemical industry press, Beijing, 2011, pp. 398–99.
4. VDEH: *Slag Atlas*, 2nd ed., Verlag Stahleisen GmbH, Düsseldorf, 1995, pp. 184–85.
5. R.C. DeVries, R. Roy, and E.F. Osborn: *Am. Ceram. Soc.*, 1955, vol. 38, pp. 158–71.
6. H.A. Fine and S. Arac: *Ironmak. Steelmak.*, 1980, vol. 4, pp. 160–66.
7. A. Ohno and H.U. Ross: *Can. Metall. Q.*, 1963, vol. 3, pp. 243–58.
8. E.F. Osborn and K.H. Gee: *Bull. Earth Miner. Sci. Exp. Stn.*, 1969, vol. 85, pp. 57–80.
9. B.J. Zhao, J. Eugene, and C.H. Hayes: *2009 CSM Annu. Meeting Proc.*, 1st ed., Metallurgical Industry Press, Beijing, 2009, pp. 438–42.
10. H.M. Liu, H. Du, and Z.P. Yang: *Acta Metall. Sin.*, 1992, vol. 28 (2), pp. B45–B49.
11. S.M. Jung and R.J. Fruehan: *ISIJ Int.*, 2001, vol. 41 (12), pp. 1447–53.
12. Y. Morizane, B. Ozturk, and R.J. Fruehan: *Metall. Mater. Trans. B*, 1999, vol. 30B, pp. 29–43.
13. J. Gran, B. Yan, and D. Sichen: *Metall. Mater. Trans. B*, 2011, vol. 42B, pp. 1008–16.
14. K. Yoshiaki, E.C. Carlos, W.C. Cramb, and I. Kuniyoshi: *ISIJ Int.*, 1998, vol. 38, pp. 348–56.
15. J. Li, Z.T. Zhang, L.L. Liu, W.L. Wang, and X.D. Wang: *ISIJ Int.*, 2013, vol. 53, pp. 1696–703.
16. D. Xiao, W.L. Wang, and B.X. Lu: *Metall. Mater. Trans. B*, 2015, vol. 46B, pp. 873–81.
17. H.M. Henaio, F. Kongoli, and K. Itagaki: *Mater. Trans.*, 2005, vol. 46, pp. 812–19.
18. Y.B. Kang and H.G. Lee: *ISIJ Int.*, 2005, vol. 45, pp. 1552–60.
19. H.M. Henaio, C. Pizarro, J.K. Front, A. Moyano, P.C. Hayes, and E. Jak: *Metall. Mater. Trans. B*, 2010, vol. 46B, pp. 1186–93.